LETTERS

An organic thyristor

F. Sawano[1], I. Terasaki[1], H. Mori[2,3], T. Mori[4], M. Watanabe[5], N. Ikeda[6], Y. Nogami[3,7] & Y. Noda[5]

Thyristors are a class of nonlinear electronic device that exhibit bistable resistance—that is, they can be switched between two different conductance states[1]. Thyristors are widely used as inverters (direct to alternating current converters) and for the smooth control of power in a variety of applications such as motors and refrigerators. Materials and structures that exhibit nonlinear resistance of this sort are not only useful for practical applications: they also provide systems for exploring fundamental aspects of solid-state and statistical physics. Here we report the discovery of a giant nonlinear resistance effect in the conducting organic salt[2] θ-(BEDT-TTF)$_2$CsCo(SCN)$_4$, the voltage-current characteristics of which are essentially the same as those of a conventional thyristor. This intrinsic organic thyristor works as an inverter, generating an alternating current when a static direct-current voltage is applied. Whereas conventional thyristors consist of a series of diodes (their nonlinearity comes from interface effects at the p-n junctions), the present salt exhibits giant nonlinear resistance as a bulk phenomenon. We attribute the origin of this effect to the current-induced melting of insulating charge-order domains, an intrinsically non-equilibrium phenomenon in the sense that ordered domains are melted by a steady flow.

The organic salt θ-(BEDT-TTF)$_2$CsCo(SCN)$_4$ is known as a charge-ordered conductor[2]. BEDT-TTF stands for bis(ethylenedithio)-tetrathiafulvalene, whose molecular structure is schematically shown in the inset of Fig. 1a. This salt is a layered material composed of conducting BEDT-TTF layers and insulating $CsCo(SCN)_4$ layers alternately stacked along the b axis. The Greek letter θ specifies the packing pattern of BEDT-TTF molecules in the conducting layer, representing a 'triangular lattice' in this case. On the triangular lattice of BEDT-TTF, one hole exists for every two molecules, which tends to be localized at low temperatures owing to Coulomb repulsion, hence the charge order[3,4]. In this particular salt, different patterns of charge order compete[5–7] and freeze inhomogeneously without any thermodynamic transitions[8,9]. Previously[10], we discovered giant nonlinear resistance in the related organic salt θ-(BEDT-TTF)$_2$CsZn(SCN)$_4$. The b-axis conductance abruptly jumped at a threshold electric field to a value 100 times larger, but its microscopic origin was left to be explored. Here we address its origin and report on the discovery of a unique phenomenon, the generation of an alternating current (a.c.) from a static direct-current (d.c.) voltage in a bulk single crystal.

Two single crystals (samples B1 and B2) were prepared using a galvanostatic anodic oxidation method. The detailed growth conditions and their characterization are described elsewhere[2]. The dimensions of B1 and B2 were $0.19 \times 0.09 \times 0.35\ mm^3$ and $0.19 \times 0.07 \times 0.52\ mm^3$, respectively, with the shortest dimension along the b axis (the interlayer direction). Using these, we can easily convert the resistance, current and voltage into resistivity, current density and electric field. However, for the sake of clear understanding, we choose to show only raw values in the present paper, because these are tightly bound to the measurement conditions, as will be shown later.

The voltage–current characteristics were measured by a two-probe method in series with a metal-oxide film resistor of known resistance (standard resistance R_{std}, see Fig. 1c) from 4.2 to 20 K in a liquid He cryostat. The contact resistance was 10–50 Ω at room temperature (300 K), more than 100 times smaller than the sample resistance below 20 K. The a.c. response was recorded by a digital oscilloscope equipped with a numerical fast Fourier transform (FFT) function.

Figure 1a shows the nonlinear resistance V_{sample}/I_{ex}, that is, the

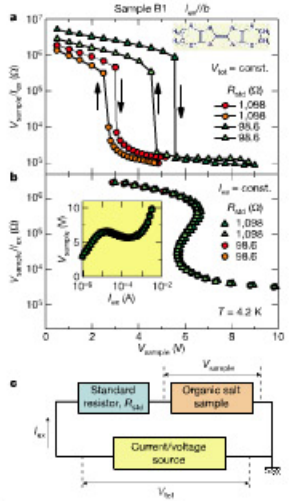

Figure 1 | Nonlinear resistance V_{sample}/I_{ex} of a θ-(BEDT-TTF)$_2$CsCo(SCN)$_4$ crystal (sample B1) at 4.2 K. The external current I_{ex} is along the b axis (interlayer direction). **a**, V_{sample}/I_{ex} measured in constant V_{tot} across the sample with a standard resistance R_{std} in series. A schematic drawing of the BEDT-TTF molecule is shown in the inset. **b**, V_{sample}/I_{ex} measured in constant external current I_{ex}. **c**, Schematic figure of the measurement configuration.

[1]Department of Applied Physics, Waseda University, Tokyo 169-8555, Japan. [2]The Institute for Solid State Physics, The University of Tokyo, Kashiwa 277-8581, Japan. [3]CREST, Japan Science and Technology Corporation, Kawaguchi 332-0012, Japan. [4]Department of Organic and Polymeric Materials, Tokyo Institute of Technology, Tokyo 152-8552, Japan. [5]Institute of Multidisciplinary Research for Advanced Materials, Tohoku University, Sendai 980-8577, Japan. [6]Japan Synchrotron Radiation Research Institute, SPring-8, Mikazuki, Hyogo 679-5198, Japan. [7]The Graduate School of Natural Science and Technology, Okayama University, Okayama 700-8530, Japan.

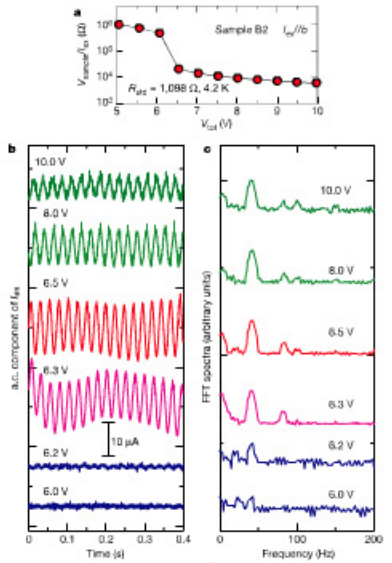

Figure 2 | Inverter (d.c.–a.c. conversion) phenomena in θ-(BEDT-TTF)$_2$CsCo(SCN)$_4$ measured at 4.2 K. a, Nonlinear resistance V_{sample}/I_{ex} of the θ-(BEDT-TTF)$_2$CsCo(SCN)$_4$ crystal (sample B1) along the b-axis direction as a function of V_{tot}. **b**, The a.c. voltage component across R_{std} for various V_{tot}. **c**, FFT spectrum of **b**.

ratio of the voltage across the sample V_{sample} to the external current I_{ex}. The data were taken at 4.2 K in constant V_{tot} conditions (see Fig. 1c), and are plotted as a function of V_{sample}. Similarly to the CsZn salt[10], V_{sample}/I_{ex} shows a drastic jump at a certain voltage as well as hysteresis. Clearly, the threshold voltage depends on R_{std}, indicating that neither the threshold voltage nor the threshold electric field is intrinsic to the sample. In contrast, as shown in Fig. 1b, V_{sample}/I_{ex} in constant I_{ex} conditions is perfectly independent of R_{std}, which strongly suggests that the constant I_{ex} conditions capture the intrinsic properties. As shown in the inset of Fig. 1b, sample B1 shows a sharp negative derivative resistance $[d(V_{sample}/I_{ex})/dI_{ex} < 0]$ for $1 \times 10^{-5}\ A < I_{ex} < 2 \times 10^{-4}\ A$. The V_{sample}–I_{ex} characteristics are essentially the same as those of thyristors, indicating that the present organic salt works as an organic thyristor—an intrinsic electronics component.

Surprisingly, sample B1 has also proved to work as a d.c.–a.c. inverter. Using the same set-up as in Fig. 1c, the a.c. voltage component across the standard resistor ($R_{std} = 1{,}098\ \Omega$) was measured in various d.c. V_{tot} values at 4.2 K. As shown in Fig. 2a, the nonlinear resistance shows an abrupt jump between $V_{tot} = 6.2$ and 6.5 V. In exactly the same V_{tot} range, a large a.c. signal of 40 Hz suddenly appears (see Fig. 2b). The observed oscillation is nearly sinusoidal and has no significant higher harmonic components except for the second-order one, as shown in the FFT in Fig. 2c. Because Fig. 1c is an equivalent set-up for current-noise

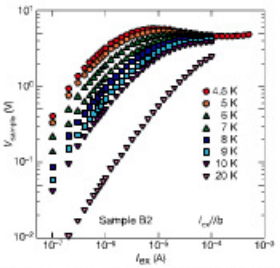

Figure 3 | Voltage–current characteristics of a second θ-(BEDT-TTF)$_2$CsCo(SCN)$_4$ crystal (sample B2) in constant external current I_{ex} at various temperatures.

measurements, the data in Fig. 2b might be called noise, but what we observed here is not noise; in this case a 40-Hz oscillation is spontaneously induced by a constant d.c. flow, as found in manufactured inverter devices.

We can understand the inverter mechanism in terms of the observed nonlinear resistance as follows. Solutions of I_{ex} for a given V_{tot} are determined graphically by an intersection of $V_{sample} = V_{tot} - R_{std}I_{ex}$ and $V_{sample} = f(I_{ex})$ in the I_{ex}–V_{sample} plane, where $f(I_{ex})$ is given by the inset of Fig. 1b. I_{ex} can take three solutions (one is unstable, the other two are stable) for a certain range of V_{tot}. In addition, we expect a capacitive component arising from the large dielectric constant[10], which shifts the phase of the time-dependent current to enable the current density oscillate in between the two stable solutions[11]. A similar oscillation has been observed in the Gunn diode at high voltages, known as the Gunn effect[12]. The oscillation period of 40 Hz is determined by the switching frequency between the low- and high-current states.

We now discuss the origin of the giant nonlinear resistance. Figure 3 shows the temperature dependence of V_{sample} in sample

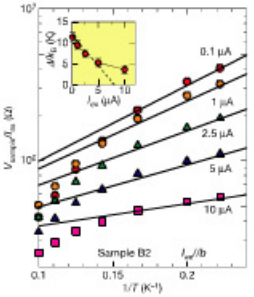

Figure 4 | Nonlinear resistance V_{sample}/I_{ex} plotted as a function of 1/T for various I_{ex}. The data are taken from Fig. 3. The solid lines are fits to an activated transport using low-temperature data (see text). In the inset the activation energy Δ evaluated from the solid lines is plotted as a function of I_{ex}. Error bars represent the ambiguity in the fits, and show ±s.d.

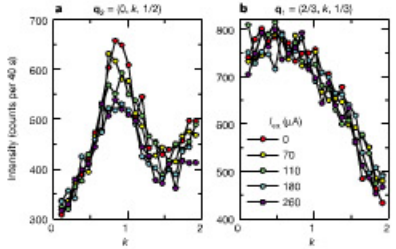

Figure 5 | Diffuse scattering intensities for θ-(BEDT-TTF)$_2$CsZn(SCN)$_4$ with various external currents applied along the *c*-axis direction at 12 K. The intensity is plotted as a function of *k* (along the *b** direction) in units of the reciprocal lattice constant. There are two diffuse streaks at $\mathbf{q}_1 = (2/3, k, 1/3)$ and $\mathbf{q}_2 = (0, k, 1/2)$ corresponding to charge order domains with different patterns. Figures 5a and b show the intensities at $\mathbf{q}_2 + \mathbf{G}_2$ and $\mathbf{q}_1 + \mathbf{G}_1$, respectively, where $\mathbf{G}_1 = (2, 1, 1)$ and $\mathbf{G}_2 = (3, 1, 0)$ are reciprocal lattice vectors chosen suitably for the measurement conditions. Whereas the $\mathbf{q}_2 + \mathbf{G}_2$ streak has a finite interlayer correlation, the $\mathbf{q}_1 + \mathbf{G}_1$ streak does not.

B2. With increasing temperature, the negative derivative resistance rapidly fades away, although the nonlinear resistance survives up to higher temperatures. At low temperatures, charge-ordered domains begin to appear. We expect the charge order to be characterized by a constant energy gap Δ, although the phase may have no long-range order. Then the charge transport should be of activation-type with an activation energy ~Δ.To include the giant nonlinear conduction effect, we allow Δ to be dependent on I_{ex}, and propose the following phenomenological expression:

$$V_{sample}/I_{ex} = R_{CO}\exp[\Delta_{I_{ex}}/k_BT] + R_N \qquad (1)$$

where R_{CO} and R_N are the resistances for the charge-ordered and conducting electrons, respectively. At low temperatures, we can safely neglect R_N, and the temperature dependence of $\Delta_{I_{ex}}$. Then V_{sample}/I_{ex} plotted on a logarithmic scale as a function of $1/T$ gives $\Delta_{I_{ex}}$, as shown in Fig. 4. The data show an upward curve, which is consistent with the temperature dependence of the resistivity of the charge-density-wave material $K_{0.3}MoO_3$ (ref. 13). This arises from a rapid growth of the gap $\Delta_{I_{ex}}$ below 20 K, and the temperature-independent $\Delta_{I_{ex}}$—that is, $\Delta(I_{ex}, T) \simeq \Delta(I_{ex}, 0)$—is only valid for $T \ll$ 20 K. We focused on the I_{ex} dependence of $\Delta_{I_{ex}}$ at 4 K, so we evaluated the magnitude of $\Delta_{I_{ex}}$ by fitting the data close to 4 K with the solid lines indicated in Fig. 4. Note that the slope, which is equal to $\Delta_{I_{ex}}/k_B$, decreases with increasing I_{ex}.

The value of Δ extracted from such analysis is plotted as a function of I_{ex} in the inset of Fig. 4. Δ/k_B for $I_{ex} \to 0$ is 13 K. This value is close to the temperature $T = 20$ K below which the resistivity rapidly increases (a signature of the growth of the charge order), thus validating to some extent our evaluation of Δ. It should be emphasized that Δ decreases roughly linearly with increasing I_{ex}, suggesting that the external current rapidly suppresses the charge order. Accordingly, negative derivative resistance can occur when the suppression of $\exp[\Delta/k_BT]$ is so rapid that $I_{ex}\exp[\Delta/k_BT]$ becomes a decreasing function of I_{ex}.

We note the following. (1) The negative derivative resistance was observed also in the in-plane (*c*-axis) direction. Thus, the voltage–current characteristics discussed here are not an interlayer effect. (2) Essentially identical voltage–current characteristics were observed in θ-(BEDT-TTF)$_2$CsZn(SCN)$_4$ along the *b*- and *c*-axis directions, which are therefore inherent to the Cs salt. Some samples showed a similar a.c. oscillation from d.c. input. (3) The measurements in (1) and (2) above were done in a four-probe configuration with a pulse current source, which indicates that the intrinsic thyristor effects are free from the contact resistance and heating effects.

Finally, to clarify the melting of the charge order by external currents, we show diffraction data under different applied currents. For the experimental requirements, we used θ-(BEDT-TTF)$_2$CsZn(SCN)$_4$ with the external current applied along the *c* direction. Figure 5 shows d.c. current dependence of the diffuse scattering intensities at $\mathbf{q}_1 = (2/3, k, 1/3)$ and $\mathbf{q}_2 = (0, k, 1/2)$ at 12 K, which correspond to different charge order domains competing with each other[5,6]. The intensity was 1,000 times weaker than that of the lattice Bragg reflection, so we used a four-circled diffractometer (wavelength $\lambda = 0.083$ nm) and synchrotron radiation as an X-ray source at BL02B1/SPring-8, Japan (details in the legend to Fig. 5). As is clearly shown, $\mathbf{q}_2$ loses its intensity with increasing current, while $\mathbf{q}_1$ remains nearly intact. The external current suppresses mainly the charge ordering with the $\mathbf{q}_2$ modulation that is responsible for the insulating behaviour[2,5,6], consistent with the current-dependent Δ in Fig. 4.

Received 20 March; accepted 27 July 2005.

1. Streetman, B. G. *Solid State Electronic Devices* 2nd edn, Ch. 11 (Prentice-Hall, Englewood Cliffs, 1980).
2. Mori, H., Tanaka, S. & Mori, T. Systematic study of the electronic state in θ-type BEDT-TTF organic conductors by changing the electronic correlation. *Phys. Rev. B* **57**, 12023–12029 (1998).
3. Seo, H. Charge ordering in organic ET compounds. *J. Phys. Soc. Jpn* **69**, 805–820 (2000).
4. Clay, R. T., Mazumdar, S. & Campbell, D. K. Charge ordering in θ-(BEDT-TTF)$_2$*X* materials. *J. Phys. Soc. Jpn* **71**, 1816–1819 (2002).
5. Nogami, Y. *et al.* Structural modulation in θ-(BEDT-TTF)$_2$CsM'(SCN)$_4$ [M' = Co, Zn]. *Synth. Met.* **103**, 1911 (1999).
6. Watanabe, M., Nogami, Y., Oshima, K., Mori, H. & Tanaka, S. Novel pressure-induced 2*k*$_F$ CDW state in organic low-dimensional compound θ-(BEDT-TTF)$_2$CsCo(SCN)$_4$. *J. Phys. Soc. Jpn* **68**, 2654–2663 (1999).
7. Mori, T. Non-stripe charge order in the θ-phase organic conductors. *J. Phys. Soc. Jpn* **72**, 1469–1475 (2003).
8. Nishio, Y. *et al.* Specific heat and metal-insulator transition of (BEDT-TTF)$_2$MZn(SCN)$_4$ (M = Cs, Rb). *Synth. Met.* **103**, 1905–1906 (1999).
9. Takahashi, T. *et al.* Charge ordering in non-dimerized BEDT-TTF based organic conductors: ^{13}C-NMR experiments. *Phys. IV Fr.* **12**(Pr9), 201–204 (2002).
10. Inagaki, K., Terasaki, I., Mori, H. & Mori, T. Large dielectric constant and giant nonlinear conduction in the organic conductor θ-(BEDT-TTF)$_2$CsZn(SCN)$_4$. *J. Phys. Soc. Jpn* **73**, 3364–3369 (2004).
11. Maeda, A., Notomi, M., Uchinokura, K. & Tanaka, S. Evidence for the existence of the inherent periodicity in the switched state at low temperatures in $K_{0.3}MoO_3$. *Phys. Rev. B* **36**, 7709–7711 (1987).
12. Gunn, J. B. Microwave oscillations of current in III–V semiconductors. *Solid State Commun.* **1**, 88–91 (1963).
13. Gruner, G. *Density Waves in Solids* 56–57 (Addison-Wesley, Reading, Massachusetts, 1994).

Acknowledgements We thank K. Inagaki for collaboration, and A. Maeda for technical advice for nonlinear-conduction and noise measurements. We also thank S. Tasaki, S. Kurihara, M. Abdel-Jawad, and N. E. Hussey for discussions. This work was partially supported by MEXT, the Grant-in-Aid for Scientific Research, and by the 21st Century COE Program at Waseda University.

Author Contributions F.S. did the electrical measurement, I.T. did the project planning and analysis, H.M. and T.M. did the sample preparation and chemical characterization, and M.W., N.I., Y.N. and Y.N. did the diffraction in electric fields.

Author Information Reprints and permissions information is available at npg.nature.com/reprintsandpermissions. The authors declare no competing financial interests. Correspondence and requests for materials should be addressed to I.T. (terra@waseda.jp).

LETTERS

Optical isotropy and iridescence in a smectic 'blue phase'

Jun Yamamoto[1,2]†, Isa Nishiyama[1], Miyoshi Inoue[1] & Hiroshi Yokoyama[1,2]

When liquid crystal molecules are chiral, the twisted structure competes with spatially uniform liquid crystalline orders, resulting in a variety of modulated liquid crystal phases, such as the cholesteric blue phase[1], twist grain boundary[2–4] and smectic blue phases[5]. Here we report a liquid crystal smectic blue phase ($SmBP_{BP}$), formed from a two-component mixture containing a chiral monomer and a 'twin' containing two repeat units of the first molecule connected by a linear hydrocarbon spacer. The phase exhibits the simultaneous presence of finite local-order parameters of helices and smectic layers, without any discontinuity on a mesoscopic length scale. The anomalous softening of elasticity due to a strong reduction in entropy caused by mixing the monomer and the twin permits the seamless coexistence of these two competing liquid crystal orders. The new phase spontaneously exhibits an optically isotropic but uniformly iridescent colour and automatically acquires spherical symmetry, so that the associated photonic band gap[6–9] maintains the same symmetry despite the local liquid crystalline order. We expect a range of unusual optical transmission properties based on this three-dimensional isotropic structure, and complete tunability due to the intrinsic softness and responsiveness of the liquid crystalline order against external fields.

We have designed a two-component mixture that consists of a chiral monomer (3B1M7) and its twin (BMHBOP-6)[10]. The twin consists of two equivalent monomer units connected by a linear hydrocarbon spacer, as shown in Fig. 1. We termed it a 'commensurate' mixture because the length of the twin is exactly twice that of the monomer. We found that mixing the twin into monomer is apparently equivalent to the introduction of connecting chains between two monomers, which freeze the motion of the monomers. There are two concentrations—ϕ_m and ϕ_t—that are equivalent to the concentrations of the monomer and (*R*,*R*) enantiomer in the twin component, respectively.

We note that six modulated phases appear in the mixture, as shown in the phase diagram (Fig. 1), but only the isotropic liquid (Iso) and smectic-A (S_A) phases appear in a pure monomer. We identified three different SmBPs—$SmBP_{X1}$, $SmBP_{X2}$ and $SmBP_{X3}$. They appear to be similar to the previously reported phases $SmBP_1$, $SmBP_2$ and $SmBP_3$, respectively[5]. We also identified a fourth smectic blue phase, $SmBP_{BP}$. A characteristic feature of $SmBP_{BP}$ is that it exhibits a completely uniform colour under a polarizing microscope without any type of macroscopic pattern or texture. Moreover, the colour does not change when the sample is rotated in any direction. This proves that $SmBP_{BP}$ has a completely isotropic optical property. It should be noted that $SmBP_{BP}$ can be detected only within a very narrow range of ϕ_m from 0.65 to 0.75. $SmBP_{X1}$ and $SmBP_{X2}$ can be distinguished clearly from $SmBP_{BP}$ by their characteristic platelet textures, as shown in Fig. 2a and b, respectively.

During the cooling process, $SmBP_{BP}$ appeared below 127 °C and was identified by the appearance of a uniform iridescent colour, as shown in Fig. 2b. The wavelength of the colour increased with a decrease in the temperature, which is a unique feature independent of both ϕ_m and ϕ_t. The platelet texture of $SmBP_{X2}$ appeared below 124 °C. During the reversible heating process, the platelet texture spontaneously melted above 124 °C, which is the temperature at which the uniform colour disappeared during the cooling process, into the uniformly coloured texture of $SmBP_{BP}$. The temperature dependence of the colour of $SmBP_{BP}$ was identical for both the cooling and heating processes, and no hysteresis was observed.

Thus, Fig. 2b provides two crucial experimental results. First, all phases ($SmBP_{X3}$, $SmBP_{BP}$ and $SmBP_{X2}$) can be proved to be thermal equilibrium phases because both phase transitions—$SmBP_{X3}$ to $SmBP_{BP}$ and $SmBP_{BP}$ to $SmBP_{X2}$—were confirmed to be thermodynamically reversible. Second, the isotropic nature of $SmBP_{BP}$ arises from an inherent feature of its internal structure, and it is not related to the existence of a polycrystalline structure during the dynamical process of phase transition. The phase transition (and colour change) is quite smooth and rapid without any time delay during the nucleation or crystal-growth processes.

Spectroscopy experiments with polarized visible light revealed that both the optical rotatory power and transmitted light intensity of the linearly polarized light in $SmBP_{BP}$ exhibited a large wavelength

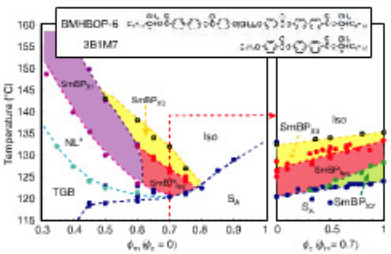

Figure 1 | Phase diagram for the twin/monomer mixture. Left, the monomer concentration (ϕ_m) dependence; right, the optical purity (ϕ_t) dependence of the twin by fixing $\phi_m = 0.7$. The TGB and NL* phases can easily be identified under a polarizing microscope because of their large optical anisotropy and characteristic patterns. The inset shows the molecular formulas of the twin (BMHBOP-6) and monomer (3B1M7).

†ERATO Yokoyama Nano-structured Liquid Crystal Project, JST, 5-9-9 Tokodai, Tsukuba 300-2635, Japan. [2]Nanotechnology Research Institute, AIST, 1-1-1 Umezono, Tsukuba 305-8568, Japan. (Present address: Department of Physics, Graduate School of Science, Kyoto University, Kitashirakawa, Sakyo, Kyoto 606-8502, Japan.